

## Atmospheric inverse estimates of methane emissions from Central California

Chuanfeng Zhao,<sup>1</sup> Arlyn E. Andrews,<sup>2</sup> Laura Bianco,<sup>2,3</sup> Janusz Eluszkiewicz,<sup>4</sup> Adam Hirsch,<sup>2,3</sup> Clinton MacDonald,<sup>5</sup> Thomas Nehrkorn,<sup>4</sup> and Marc L. Fischer<sup>1</sup>

Received 23 December 2008; revised 2 April 2009; accepted 8 June 2009; published 25 August 2009.

[1] Methane mixing ratios measured at a tall tower are compared to model predictions to estimate surface emissions of CH<sub>4</sub> in Central California for October–December 2007 using an inverse technique. Predicted CH<sub>4</sub> mixing ratios are calculated based on spatially resolved a priori CH<sub>4</sub> emissions and simulated atmospheric trajectories. The atmospheric trajectories, along with surface footprints, are computed using the Weather Research and Forecast (WRF) coupled to the Stochastic Time-Inverted Lagrangian Transport (STILT) model. An uncertainty analysis is performed to provide quantitative uncertainties in estimated CH<sub>4</sub> emissions. Three inverse model estimates of CH<sub>4</sub> emissions are reported. First, linear regressions of modeled and measured CH<sub>4</sub> mixing ratios obtain slopes of  $0.73 \pm 0.11$  and  $1.09 \pm 0.14$  using California-specific and Edgar 3.2 emission maps, respectively, suggesting that actual CH<sub>4</sub> emissions were about  $37 \pm 21\%$  higher than California-specific inventory estimates. Second, a Bayesian “source” analysis suggests that livestock emissions are  $63 \pm 22\%$  higher than the a priori estimates. Third, a Bayesian “region” analysis is carried out for CH<sub>4</sub> emissions from 13 subregions, which shows that inventory CH<sub>4</sub> emissions from the Central Valley are underestimated and uncertainties in CH<sub>4</sub> emissions are reduced for subregions near the tower site, yielding best estimates of flux from those regions consistent with “source” analysis results. The uncertainty reductions for regions near the tower indicate that a regional network of measurements will be necessary to provide accurate estimates of surface CH<sub>4</sub> emissions for multiple regions.

**Citation:** Zhao, C., A. E. Andrews, L. Bianco, J. Eluszkiewicz, A. Hirsch, C. MacDonald, T. Nehrkorn, and M. L. Fischer (2009), Atmospheric inverse estimates of methane emissions from Central California, *J. Geophys. Res.*, 114, D16302, doi:10.1029/2008JD011671.

### 1. Introduction

[2] Changes in atmospheric methane play an essential role in Earth’s climate. CH<sub>4</sub> is now associated with a direct radiative forcing of  $\sim 0.48 \text{ W m}^{-2}$  [IPCC, 2007] and an indirect radiative forcing of  $\sim 0.13 \text{ W m}^{-2}$  [Lelieveld *et al.*, 1998], which accounts for about  $\frac{1}{2}$  of the non-CO<sub>2</sub> radiative forcing ( $0.98 \text{ W m}^{-2}$  in 2004 [Hofman *et al.*, 2006]) and about  $\frac{1}{4}$  of the total radiative forcing ( $2.64 \text{ W m}^{-2}$  from IPCC [2007]) from all greenhouse gases (GHGs). It has been argued that reducing anthropogenic emissions of methane may be an important component of an initial strategy for avoiding the most severe impacts of global

warming [Hansen *et al.*, 1998; Hansen, 2004; Shindell *et al.*, 2005]. In particular, reduction of anthropogenic methane emissions may be possible (e.g., improving CH<sub>4</sub> recovery from landfills and waste treatment, reducing industrial emissions, and improving agricultural practices) [Harriss, 1994]. In view of methane’s role in the climate system, increased attention has been brought recently to assessing CH<sub>4</sub> sources [Gimson and Uliasz, 2003; Miller and Tans, 2003; Houweling *et al.*, 2006; Kort *et al.*, 2008].

[3] In California, total GHG emissions in 2004 were approximately 480 MMT CO<sub>2</sub> equivalent, with CH<sub>4</sub> contributing approximately 6% [CARB, 2007]. Now that California has passed Assembly Bill 32, which requires that greenhouse gases emissions be reduced to 1990 levels by 2020, careful accounting of current CH<sub>4</sub> emissions and of their future reductions is essential. Unfortunately, current inventory and model-based estimates of CH<sub>4</sub> emissions are uncertain because many of the factors controlling emissions are poorly quantified. Atmospheric measurements and inverse modeling may provide an independent method to quantify local to regional CH<sub>4</sub> emissions from California.

[4] Atmospheric inverse methods to estimate the surface CH<sub>4</sub> fluxes from in situ and remotely sensed CH<sub>4</sub> mixing

<sup>1</sup>Environmental Energy Technology Division, Lawrence Berkeley National Laboratory, Berkeley, California, USA.

<sup>2</sup>Earth System Research Laboratory, NOAA, Boulder, Colorado, USA.

<sup>3</sup>Cooperative Institute for Research in Environmental Sciences, University of Colorado, Boulder, Colorado, USA.

<sup>4</sup>Atmospheric and Environmental Research, Inc., Lexington, Massachusetts, USA.

<sup>5</sup>Sonoma Technology, Inc., Petaluma, California, USA.

ratio measurements and modeled wind fields have been widely applied at both global and regional scales [Hein *et al.*, 1997; Houweling *et al.*, 1999; Vermeulen *et al.*, 1999; Bergamaschi *et al.*, 2000, 2005, 2007; Dentener *et al.*, 2003; Gimson and Uliasz, 2003; Manning *et al.*, 2003; Mikaloff Fletcher *et al.*, 2004a, 2004b; Chen and Prinn, 2006; Kort *et al.*, 2008]. In general, the components of atmospheric inverse emission estimates are CH<sub>4</sub> mixing ratio measurements, an atmospheric transport model (including chemistry for global simulations), in some cases a priori estimates for CH<sub>4</sub> emissions and sinks or their correlation structure, and a statistical technique to minimize differences between measured and predicted CH<sub>4</sub> mixing ratios. To estimate CH<sub>4</sub> emissions and their associated uncertainties, errors from each of these components should be accounted for and formally propagated through the inversion process.

[5] In this study, we employ an approach originally developed to estimate regional CO<sub>2</sub> emissions [Gerbig *et al.*, 2003a, 2003b] that combines calculation of surface footprints [Lin *et al.*, 2004] with procedures to estimate transport model uncertainty [Lin and Gerbig, 2005] using the Stochastic Time-Inverted Lagrangian Transport (STILT) model. Of particular relevance to our work, Kort *et al.* [2008] recently used observations of CH<sub>4</sub> and N<sub>2</sub>O from an airborne platform in combination with STILT to infer CH<sub>4</sub> and N<sub>2</sub>O emissions from the continental interior of North America in May–June 2003. Our study also uses STILT, but applies it to a smaller model domain at finer spatial and temporal resolutions, taking advantage of unique computational benefits offered by the Lagrangian approach.

[6] To address the problem of estimating CH<sub>4</sub> emissions from different sources in Central California, we conducted coordinated CH<sub>4</sub> measurements and modeling as part of the California Greenhouse Gases Emission Measurement (CALGEM) project. Section 2 describes the methods for the measurements of CH<sub>4</sub> mixing ratios, profiler-based estimates of wind fields and boundary layer heights, spatially resolved a priori CH<sub>4</sub> emission maps, meteorological transport fields and resulting surface footprints, an analysis of measurement and model errors, and the Bayesian inverse model used to estimate CH<sub>4</sub> emissions. Section 3 describes the results of the measurements, bias corrections and error estimates, and the best estimates of CH<sub>4</sub> surface emissions implied by the measurements. Section 4 discusses the estimates of CH<sub>4</sub> emissions in the context of current inventories, examines the spatial region in which the tower measurements effectively constrain CH<sub>4</sub> emissions, and concludes with initial recommendations for additional measurement sites to constrain other important emission regions in California.

## 2. Data and Methods

### 2.1. CH<sub>4</sub> Measurements

[7] The CH<sub>4</sub> measurements were made at 91 and 483 m on a tall tower near Walnut Grove, CA (WGC, 121.49°W, 38.27°N, 0 m above sea level), beginning in September 2007. The measurements were made using a sampling and analysis system combining pumps, air driers, and three gas analyzers. Briefly, air samples are drawn continuously from the different heights on the tower, are partially dried by a condensing system that lowers water vapor to a 5°C dew

point, are sequentially applied on a 5 minute interval to a temperature stabilized membrane drier (Purmapure Inc.) which dries air to a –33°C dew point, and then are supplied to the gas analyzers. The first 4.5 minutes of each measurement interval are used to allow equilibration of the gas concentrations and instrument response, while the last 30 seconds is used as the measurement interval. In particular, CH<sub>4</sub> is measured using a cavity ring-down spectrometer (Picarro EnviroSense 3000i) with an accuracy and precision of approximately 0.3 ppb in the 30 second averaging interval. To quantify and correct instrument drifts, the offset is measured and corrected every ½ hour using a reference gas, while the gain (and linearity) is checked and corrected every 6 hours using 4 NOAA gas primary standards. In addition, flask samples were collected twice daily (1000 and 2200 hr GMT) from a separate sample line at the 91 m level and analyzed at NOAA-ESRL. To provide additional quality assurance, the in situ CH<sub>4</sub> measurements were compared with the flask measurements. This redundancy allows the detection of small (~ppb) sampling errors. In general, the difference between in situ and flask analyses was consistent with the precision of the in situ instrument. During some periods, particularly during late night and early morning, variability in CH<sub>4</sub> mixing ratios was larger. For these periods, the difference between flask the in situ CH<sub>4</sub> measurements was generally consistent with the standard deviation of the in situ CH<sub>4</sub> measurements averaged over a 30 minute window centered on the flask sample.

[8] Figure 1 shows 3-hour averages of measured CH<sub>4</sub> mixing ratios at 91 m (black) and 483 m (red) in October 2007. Diurnal cycles due to changing boundary layer height are apparent in the data. The daily maximum CH<sub>4</sub> mixing ratio measured at 91 m often occurs when the minimum is obtained at 483 m. This would be expected to occur in cases when the boundary layer lies between 91 and 483 m, trapping surface emissions within a shallow layer that is measured by 91 m sample height, while the 483 m sample height observes comparatively decoupled background air. In the following work, we will use the daily minimum CH<sub>4</sub> measurements at 483 m to provide a check on the CH<sub>4</sub> background analysis. Moreover, we limited the inverse model study to only include measurements collected during well-mixed periods. Henceforth, we define the well-mixed periods by using the criteria that the difference of measurements at 91 m and 483 m are less than 100 ppb, as shown by the black points in Figure 1. This criteria will also be evaluated in the following analysis.

### 2.2. Wind Profiler Measurements

[9] To quantify uncertainties in modeled atmospheric transport, hourly boundary layer heights and vertical profiles of winds were obtained from a radar wind profiler (RWP) operated by the Sacramento Metropolitan Air Quality Management District. The profiler is located (38.30°N, 121.42°W) within 8 km of the tower used for the CH<sub>4</sub> measurements. Given the level terrain of the Sacramento delta region, we expect that errors in modeled winds and PBL heights for the region surrounding the tower can be accurately assessed by comparing the wind profiler measurements with corresponding meteorological simulations for profiler (winds) and tower (PBL) locations. The RWP acquires data in two different settings, high-resolution and

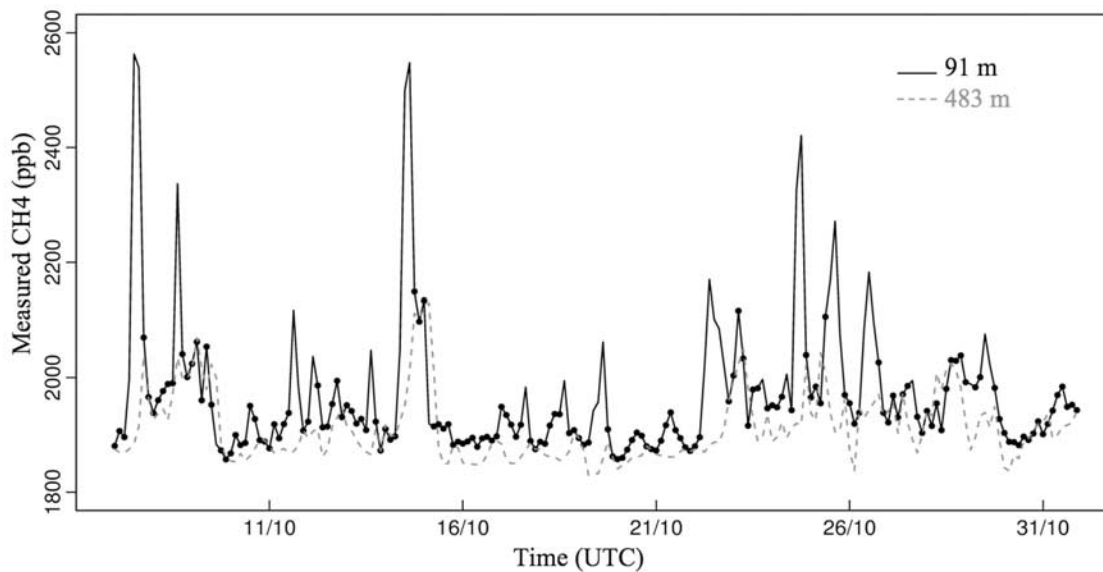


**Figure 1.**  $\text{CH}_4$  mixing ratios measured at 91 m (black) and 483 m (gray) at the WGC tower. Only data (black points) obtained during well-mixed periods (defined as when the difference between measurements at 91 and 483 m are less than 100 ppb) are used in this study.

low-resolution mode with vertical resolutions of 60 m and 105 m respectively. Boundary layer heights were estimated from subhourly RWP vertical velocity and returned signal strength (signal-to-noise ratio) data using objective algorithms and qualitative analysis following techniques found in the works of Wyngaard and LeMone [1980], Bianco and Wilczak [2002], and Bianco *et al.* [2008]. In the used configuration, the RWP can detect boundary layer heights from about 150 m to 4000 m with an accuracy of  $\pm 200$  m [Dye *et al.*, 1995].

### 2.3. The a Priori $\text{CH}_4$ Emissions

[10] We used two methods to estimate  $\text{CH}_4$  emissions. As a base case, we used the North American maps of total anthropogenic  $\text{CH}_4$  from the EDGAR 3.2 model with  $1 \times 1$  degree spatial resolution [Olivier *et al.*, 2005]. To provide finer spatial resolution inside California, we also estimated California  $\text{CH}_4$  emissions separately for six source sectors: landfills (LF), livestock (LS), natural gas production and use (NG), petroleum refining (PL), crop agriculture (CP), and wetlands (WL).  $\text{CH}_4$  emissions from landfills were estimated by the California Air Resources board (L. Hunsaker, private communication, 2008) using IPCC methods [IPCC, 2006], which is driven by landfill specific waste application statistics from the CA Waste Management Board [e.g., Carr, 2004] and site-specific estimates of  $\text{CH}_4$  recovery.  $\text{CH}_4$  from livestock was estimated using United States Department of Agriculture (USDA) county level animal stocking densities [Census, 2002] and animal specific emission factors for dairy and beef cattle separately [Franco, 2002].  $\text{CH}_4$  from natural gas production and use and from petroleum refining activities were estimated as the difference of total minus reactive hydrocarbon (typically between 0.2 and 0.4 of the total) emissions estimated from the California Air Resources Board (CARB) emission criteria pollutant emission inventory for those source sectors (<http://www.arb.ca.gov/app/emsinv/fcemssumcat2006.php>).  $\text{CH}_4$  emis-

sions from crop agriculture were assumed to follow emissions from the DNDC model for an average climate year with high irrigation as described by Salas *et al.* [2006].  $\text{CH}_4$  emissions from wetlands were assumed to follow the National Aeronautics and Space Administration Carnegie-Ames-Stanford Approach (NASA-CASA) estimates from Potter *et al.* [2006]. Although some of these sources are expected to vary on a seasonal basis, we calculated mean emissions and did not attempt to resolve temporal variations over the relatively short period of this three months study. Maps of the a priori  $\text{CH}_4$  emissions are shown in Figures 2a–2f for these six California-specific source sectors. For comparison, Figure 2g shows total EDGAR 3.2 emissions for the Western United States, while Figure 2h shows the sum of the California-specific  $\text{CH}_4$  emissions. Last, Figure 2i shows a set of California subregions that roughly correspond to air basins that are nearby or distant from the measurement locations and will be used in following analysis. Table 1 summarizes the  $\text{CH}_4$  emissions from different California-specific sources in the 13 subregions.  $\text{CH}_4$  emissions are scaled to equivalent  $\text{CO}_2$  forcing using a global warming potential of 25 ( $\text{gCO}_{2\text{eq}} \text{gCH}_4^{-1}$  [IPCC, 2007]). The total of the California-specific emissions is similar to total  $\text{CH}_4$  emissions ( $\sim 31 \text{ MMT CO}_{2\text{eq}}$ ) reported by the California Air Resource Board [CARB, 2007], but is approximately half the total emissions from California pixels in the Edgar 3.2 inventory. Inspection of the Edgar 3.2 emissions shows that the largest sources are from natural gas ( $22.5 \text{ MMT CO}_{2\text{eq}}$ ) and landfills ( $19.3 \text{ MMT CO}_{2\text{eq}}$ ), suggesting very different assumptions about emissions from these sources. To assign an uncertainty to the a priori emissions, we follow previous work on uncertainty analysis [USEPA, 2004; Farrell *et al.*, 2005] and assign a 30% uncertainty to each of emissions sources. We consider the uncertainties in US total  $\text{CH}_4$  emissions only a rough estimate to the uncertainties for subregions of California (and over the time period of this study)

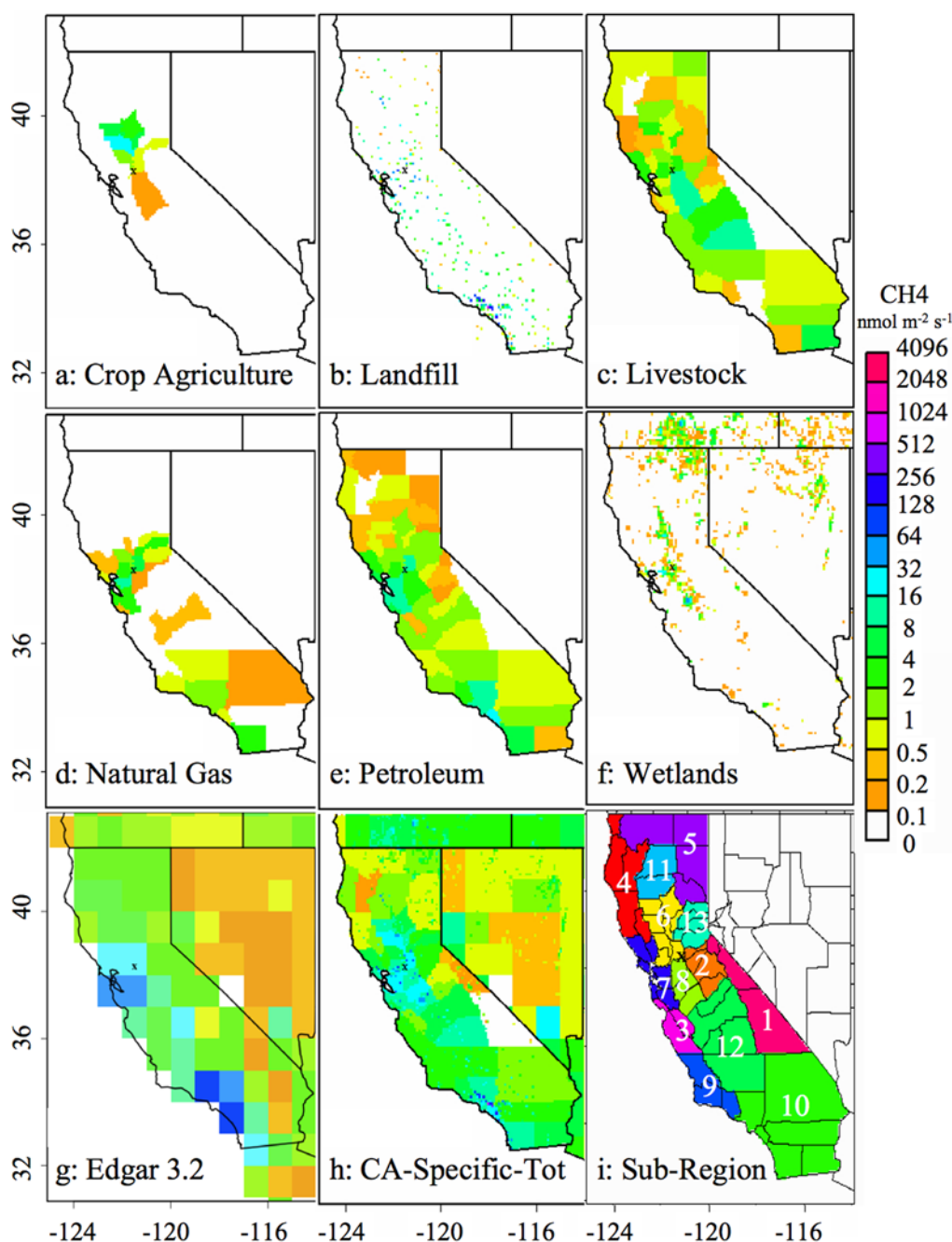


**Figure 2.** The a priori emission maps and regions in California. (a–f) The CA-specific surface CH<sub>4</sub> emissions from different sources. (g) Anthropogenic surface CH<sub>4</sub> emissions from Edgar 3.2. (h) The sum of maps of Figures 2a–2f specific to California. (i) An illustration of the 13 California subregions considered in the region analysis. The tower location is marked with a “x”.

because the 30% estimate was derived for more aggregated emissions over annual cycles and the entire continental US.

#### 2.4. WRF-STILT Model

[11] As mentioned in the Introduction, the work presented in this paper employs the STILT model, run in the time-reversed (receptor-oriented) mode, as the atmospheric transport model. STILT is a Lagrangian Particle Dispersion Model (LPDM) that has been specifically developed and applied to regional simulations and inverse flux estimates

for CO<sub>2</sub>, other greenhouse gases, and CO. Its detailed description is provided elsewhere [Lin *et al.*, 2003, 2004; Gerbig *et al.*, 2003a; Matross *et al.*, 2006; Kort *et al.*, 2008; Miller *et al.*, 2008] and, consequently, only the most pertinent features will be summarized here. As in all LPDMs, transport in STILT includes both advective and turbulent components, with turbulence being responsible for the dispersion of particles. In this application, given input meteorological data, the STILT model transports ensembles of 100 particles (air parcels) backward in time 5 days for a

**Table 1.** A Priori CH<sub>4</sub> Emissions (MMT CO<sub>2eq</sub>) From Six Different Sources and 13 California Regions in Figure 2i

CH <sub>4</sub> (MMT CO <sub>2eq</sub> )	CP	LF	LS	NG	PL	WL	CA-specific	Edgar3.2
Region 01	0.04	0.02	0.04	0.00	0.02	0.06	0.18	0.92
Region 02	0.01	0.04	0.15	0.00	0.10	0.02	0.29	1.09
Region 03	0.01	0.05	0.20	0.01	0.20	0.02	0.45	1.74
Region 04	0.04	0.10	0.18	0.00	0.17	0.05	0.48	1.56
Region 05	0.05	0.02	0.39	0.00	0.11	0.07	0.57	1.76
Region 06	0.02	0.40	0.51	0.36	0.62	0.04	1.81	4.30
Region 07	0.01	0.74	0.31	0.67	1.50	0.02	3.25	5.95
Region 08	0.01	0.27	2.06	0.01	0.32	0.02	2.32	3.73
Region 09	0.02	0.26	0.24	0.13	0.37	0.02	0.96	3.48
Region 10	0.11	3.75	1.68	0.88	3.62	0.17	10.21	25.14
Region 11	0.02	0.13	0.19	0.01	0.10	0.02	0.47	1.09
Region 12	0.06	0.31	3.65	0.31	0.73	0.10	5.16	7.95
Region 13	0.01	0.06	0.06	0.19	0.19	0.02	0.53	1.07
Whole CA	0.42	6.15	9.66	2.57	8.03	0.63	27.46	59.78

receptor point (WGC site here). We calculate the response of the target gas concentration at the receptor point to surface sources (“footprint”), in units of ppb/(nmol m<sup>-2</sup> s<sup>-1</sup>). The footprint, which represents the adjoint of the transport field, is calculated by counting the number of particles in a surface-influenced region (defined as 1/2 of the estimated PBL height in the STILT model, for example, see *Gerbig et al.* [2003a] and *Kort et al.* [2008]) and the time spent in the region (for details, see *Lin et al.* [2003]). When multiplied by the a priori field of surface flux, the footprint gives the associated contribution to the mixing ratio measured at the receptor, hence the footprints can be used to estimate parameters of the source functions and their respective uncertainties.

[12] We calculate the footprints relating surface fluxes to measured CH<sub>4</sub> mixing ratios using the meteorological output from a customized version of the Weather Research and Forecasting model [*Skamarock et al.*, 2005] to drive STILT. This combined model will henceforth be referred to as WRF-STILT. Specifically, the WRF model version 2.2 has been modified to output time-averaged (hourly in this study) values of the mass-coupled velocities, which significantly improve mass conservation in STILT (compared with the instantaneous advective velocities), as well as convective mass fluxes that are used directly in the STILT calculations. The main physical options are set as following: (1) Radiation: RRTM scheme [*Mlawer et al.*, 1997] for the longwave and Goddard scheme [*Chou and Suarez*, 1994] for the shortwave; (2) Planetary Boundary Layer: Yonsei University (YSU) scheme coupled with the NOAH land surface model and the MM5 similarity theory based surface layer scheme. (3) Microphysics: Purdue Lin scheme [*Lin et al.*, 1983; *Chen and Sun*, 2002] (4) Convection: Grell-Devenyi ensemble mass flux scheme [*Grell and Devenyi*, 2002]. The initial and boundary meteorology conditions for WRF are provided by the North American Regional Reanalysis (NARR [*Mesinger et al.*, 2006]). A one-way nesting WRF running with 3 nest levels is used for the meteorology simulations around the WGC tower location, which is shown in Figure 3 (Domain 1:  $-149.16^\circ < \text{lon} < -102.21^\circ$ ,  $17.82^\circ < \text{lat} < 50.53^\circ$  on a 40 km grid; Domain 2:  $-123.53^\circ < \text{lon} < -120.66^\circ$ ,  $36.76^\circ < \text{lat} < 38.94^\circ$  on a 8 km grid; Domain 3:  $-121.71^\circ < \text{lon} < -121.23^\circ$ ,  $38.09^\circ < \text{lat} < 38.45^\circ$  on a 1.6 km grid). The vertical

resolution is taken from the input meteorology from NARR with 30 layers. Each day was simulated separately using 30-hour run (including 6 hours from the previous day for spin-up) with hourly output. Growth in transport model errors were minimized by nudging the forecast fields to the gridded NARR analysis fields every 3 hours.

## 2.5. WRF-STILT Transport Errors

[13] As a first approximation to evaluate the transport errors in the WRF-STILT predictions of surface influence footprints, we compared the modeled estimates of WRF winds and WRF-STILT boundary layer heights ( $Z_i$ ) with corresponding profiler measurements of wind velocity and  $Z_i$ . Errors in modeled winds are estimated by comparing WRF predictions with profiler measurements of the  $u$  and  $v$  wind components at a height of 137 m, close to the height of the air sampling. Using data from the October to December 2007, the root mean square (RMS) errors in horizontal winds at 137 m are 2.21 ( $\sigma_u$ ) and 2.86 m s<sup>-1</sup> ( $\sigma_v$ ) for the

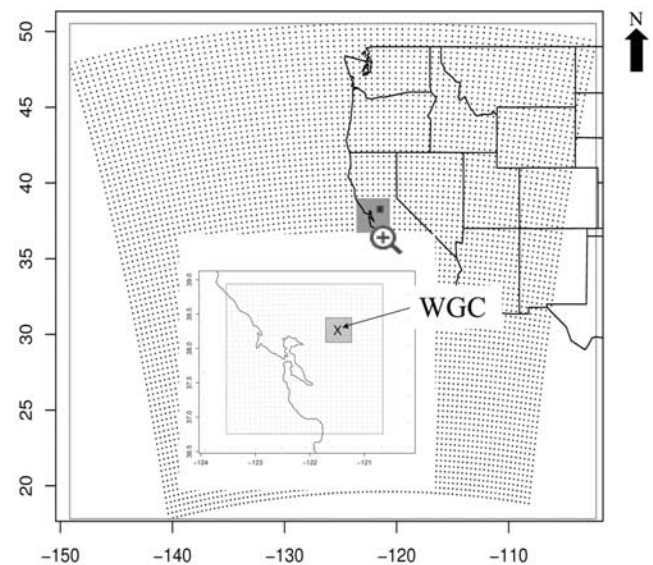


**Figure 3.** Map grids showing the three model domains used in the meteorological predictions and WGC tower location “X” ( $-121.49, 38.26$ ) of the measurements.

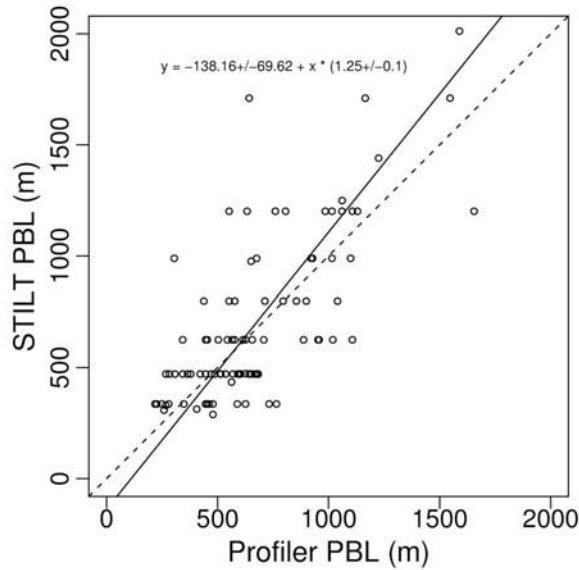


**Figure 4.** Comparison of well-mixed daytime PBL heights between radar profiler measurements and WRF-STILT simulations in October through December 2007.

u and v directions respectively. Some of this difference can be attributed to the fact that profiler winds are measured at a single site while the WRF winds are the averages over a grid of  $1.6 \times 1.6$  km. We note that the RMS error decreased by approximately a factor of 2 between 137 m and 1000 m above the ground, though the decrease was nonlinear with most of the decrease occurring between 137 and about 500 m. Henceforth, we assume errors in u and v are constant with height and randomly distributed with an RMS magnitude of  $3.6 \text{ m s}^{-1}$ , which is obtained as  $\sigma_v = \sqrt{\sigma_u^2 + \sigma_v^2}$ .

[14] Measured and predicted daytime boundary layer heights in October through December 2007 are shown in Figure 4. Profiler data were selected to match the time of the WRF predictions to within 1 hour. In addition, the WRF-STILT simulations impose a lower limit value of 215 m on  $Z_i$ , while the radar profiler has a minimum detection height of 120 m. To avoid biasing the comparison and make sure  $\text{CH}_4$  well mixed from surface till heights above 483 m, we included WRF-STILT predictions of  $Z_i$  greater than 215 m in the analysis. The resulting best fit geometric linear regression of WRF-STILT on radar profiler PBL heights yields a slope of  $1.25 \pm 0.10$  and intercept of  $-138 \pm 70$  m. Based on this result, we obtain a scale factor of  $1/1.25$  which is then applied to  $Z_i$  when calculating footprints using STILT. This result is similar to that found in the work of Lin *et al.* [2003], where STILT predictions of  $Z_i$  were about 1.09 higher than  $Z_i$  measurements at a site in Wisconsin. After scaling STILT  $Z_i$  by a factor of  $1/1.25$ , the RMS residual error between scaled WRF-STILT and profiler  $Z_i$  is reduced by a factor of 1.5 to  $\sim 200$  m, roughly consistent with the estimated error in the profiler measurements. In the following work we calculate particle trajectories and resulting footprints using the scaled parameterization of PBL height. It is possible that an additional error in the effective wind field may be introduced by the  $Z_i$  scaling for particles near the top of the boundary layer if

there is significant wind shear at that altitude but expect that this is small compared to the first order errors already identified for winds and PBL heights.

## 2.6. Footprints and Predicted $\text{CH}_4$ Signals

[15] Particle trajectories were calculated using STILT driven by the WRF winds. One hundred particles are released every 3 hours (from UTC hour 00) at the WGC tower and transported backward in time 5 days to insure a majority of the particles reach positions representative of the marine boundary layer. Footprints are then calculated from the particle trajectories as in the work of Lin *et al.* [2004]. The time-averaged footprint is shown in Figure 5 for the period between October and December in 2007. The high footprint values within approximately the Central California area near the tower site indicate that  $\text{CH}_4$  signals measured at 91 m and 483 m at WGC will be strongly influenced by the California emissions.

[16] Predicted local  $\text{CH}_4$  signals  $C_l(\underline{X}_r, t_r)$  (index “l” denote local and “r” denote receptor) from land surface emissions are calculated using the product of the footprint maps and the a priori emission maps, as

$$C_l(\underline{X}_r, t_r) = \sum_{i,j,m} f(\underline{X}_r, t_r | x_i, y_j, t_m) \cdot F(x_i, y_j), \quad (1)$$

where  $\underline{X}_r$  and  $t_r$  are receptor (WGC tower) location and time,  $f(\underline{X}_r, t_r | \underline{X}, t_m)$  is the footprint and  $F(x_i, y_j)$  is the surface emission map at location  $(x_i, y_j)$  and time  $t_m$ . The total  $\text{CH}_4$  mixing ratio at the receptor can be expressed as

$$C(\underline{X}_r, t_r) = C_l(\underline{X}_r, t_r) + C_{BG}(\underline{X}_r, t_r), \quad (2)$$

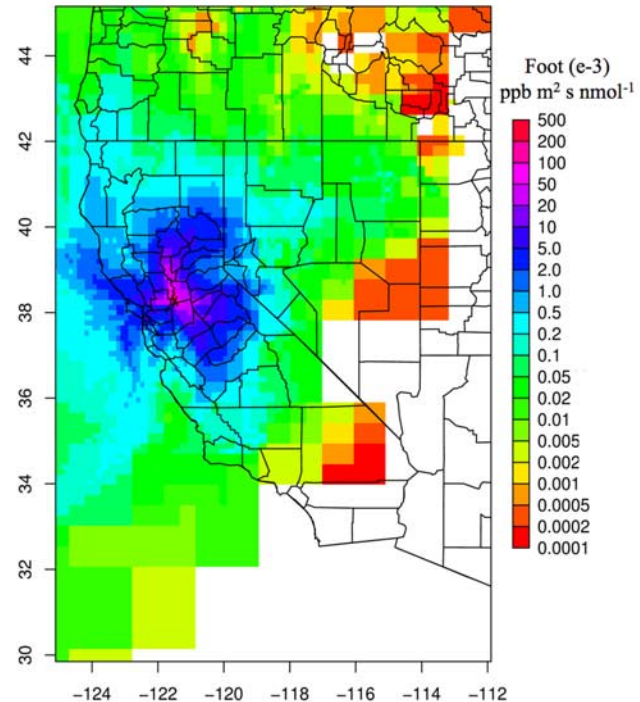


**Figure 5.** Averaged footprints for mixing ratio measurements made at the tower location “X” ( $-121.49, 38.26$ ).

where  $C_{BG}(\underline{X}_r, t_r)$  is the upstream CH<sub>4</sub> background mixing ratios.

## 2.7. Inversion Technique

[17] The *posterior* CH<sub>4</sub> emissions were estimated by optimizing scaling factors for the *a priori* CH<sub>4</sub> emissions to provide a best fit between measured and predicted CH<sub>4</sub> mixing ratios. This was done in two ways: (1) as a standard least square optimization of an overall scaling factor for all land surface emissions and (2) in a Bayesian approach that scales each source type or subregion separately and incorporates individual estimates for the uncertainties in different *a priori* emissions.

[18] Combining equations (1) and (2), the difference between measured and predicted background CH<sub>4</sub> relates to the surface emission flux as

$$\underline{C} - \underline{C}_{BG} = \underline{f}F, \quad (3)$$

where  $\underline{f}$  is footprints,  $F$  is surface CH<sub>4</sub> emission,  $\underline{C}$  and  $\underline{C}_{BG}$  is CH<sub>4</sub> mixing ratios from tower measurements and background calculations, respectively. Assuming mixing ratio measurements from local sources as  $y = \underline{C} - \underline{C}_{BG}$ . Following Gerbig *et al.* [2003a], we introduce a model parameter or a state vector of scaling factors,  $\lambda$ , for the surface flux,  $F(\lambda)$ . The inversion adjusts the model parameters  $\lambda$  such that the modeled changes in CH<sub>4</sub> concentrations are optimally consistent (in standard least square sense) with the observed values. In the study of surface CH<sub>4</sub> emissions from different sources (“source analysis” hereafter),  $\lambda$  represents the scaling factor for different sources; in the study of surface CH<sub>4</sub> emissions from different regions (“region analysis” hereafter),  $\lambda$  represents the scaling factor for different areas. For both the “source analysis” and “region analysis” study,  $F(\lambda)$  is linearly dependent on  $\lambda$ :

$$F(\lambda) = \underline{\phi}\lambda \quad (4)$$

where  $\underline{\phi}$  is the *a priori* emissions for different sources or regions in this study.

[19] Using the same method as by Lin *et al.* [2004], the analytical solutions to equations (3) and (4) are

$$\begin{aligned} \hat{\lambda} &= (\underline{K}^T \underline{S}_\varepsilon^{-1} \underline{K})^{-1} (\underline{K}^T \underline{S}_\varepsilon^{-1} \underline{y} + \underline{S}_{prior}^{-1} \lambda_{prior}) \\ \hat{\underline{S}}_\lambda &= (\underline{K}^T \underline{S}_\varepsilon^{-1} \underline{K} + \underline{S}_{prior}^{-1})^{-1} \end{aligned} \quad (5)$$

where  $\underline{K} = \underline{f}\underline{\phi}$ ,  $\underline{S}_\varepsilon$  is measurement error covariance matrix  $\lambda_{prior}$  and  $\hat{\lambda}$  are the *a priori* and *a posteriori* vectors, and  $\underline{S}_{prior}$  and  $\hat{\underline{S}}_\lambda$  are the *a priori* and *a posteriori* error matrices for  $\lambda$ . Corresponding to our initial estimate of 30% uncertainty in the CH<sub>4</sub> emission maps, the initial value of  $\underline{S}_{prior}$  is 0.09. Note that the measurements and *a priori* emission error matrices are diagonal, equivalent to assuming that the prior errors are uncorrelated. The measured and predicted CH<sub>4</sub> signals are computed and compared on a 3 hour interval.

## 2.8. Error Covariance Matrix

[20] The equivalent “measurement” error covariance matrix  $\underline{S}_\varepsilon$  is formed as the sum of different components

$$\begin{aligned} \underline{S}_\varepsilon &= \underline{S}_{part} + \underline{S}_{aggr} + \underline{S}_{TransWND} + \underline{S}_{TransPBL} + \underline{S}_{bkgd} \\ &\quad + \underline{S}_{eddy} + \underline{S}_{ocean} \end{aligned} \quad (6)$$

Here as in the work of Lin *et al.* [2004], the contribution of instrumentation error in the CH<sub>4</sub> measurements is assumed to be random, uncorrelated, and negligible in magnitude relative to the other sources of error, and hence not considered further in the inverse model estimates. We consider each of the terms in equation (6) below.

[21] The particle number error ( $S_{part}$ ) is due to the finite number of released particles at the receptor location. It can be estimated by comparing the simulated signals from the STILT running with release of 1000 particles and those from the STILT running with release of 100 particles. Using the WRF simulated meteorology in October 2007 and the total *a priori* emission map, we found that the standard error is about 3 ppb, indicating ~5% particle number error. This value is less than ~13% particle number error for CO<sub>2</sub> indicated by Gerbig *et al.* [2003a]. Considering the ~5% error determined by us here and ~13% error determined by Gerbig *et al.* for signals in the mixed-layer,  $S_{part}$  for 100 particles is assumed as 10% in this study. For all of the following error analyses, we used 1000 particles in order to minimize the effect of particle number error.

[22] The “aggregation error” ( $S_{aggr}$ ) arises from aggregating heterogeneous fluxes within a grid cell into a single average flux [Kaminski *et al.*, 2001]. Gerbig *et al.* [2003b] demonstrated that a rough estimate of the aggregation error can be derived from the observed “representation error,” which is derived from the difference between a point observation and a value averaged over a specific grid size [Gerbig *et al.*, 2003a]. Without multiple observation stations over a specific grid, we try to estimate the aggregation error based on the *a priori* CH<sub>4</sub> emissions. Although we do not have high-resolution emission maps for all of the CH<sub>4</sub> sources, we estimate aggregation error using landfill emissions, which are fully resolved. Here the aggregation error is estimated by comparing the unaggregated landfill signal from the landfill signal estimated after averaging emissions over each county (the maximum aggregation used for the other sources). The average aggregation error, estimated as the RMS difference between the unaggregated and aggregated signals, is 11% of the mean landfill signal.

[23] The transport error ( $\underline{S}_{Trans} = \underline{S}_{TransWND} + \underline{S}_{TransPBL}$ ) denotes the errors in modeling transport, which can be caused by the uncertainties in wind speeds and directions, and the uncertainties in PBL heights. Following Lin and Gerbig [2005], the transport error due to winds  $\underline{S}_{TransWND}$  is calculated as the RMS difference between signals predicted from simulations with and without input of an additional stochastic component of wind error  $\sigma_V$  (3.6 m/s; section 2.5) in STILT. The resulting RMS signal is equivalent to 8% of the average predicted CH<sub>4</sub> signal. This estimate of uncertainty assumes that the wind error at the radar profiler location can be used to represent the wind error within the modeling domain. While we have not

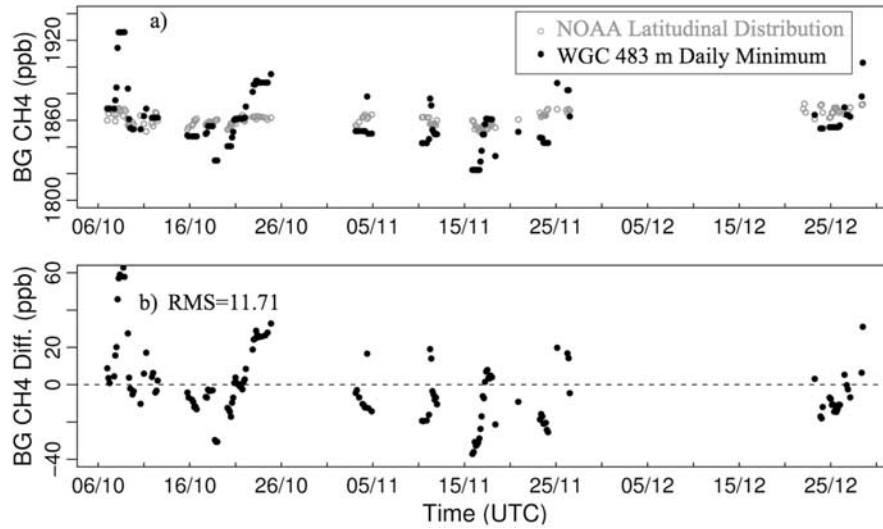


**Figure 6.** Time series of background  $\text{CH}_4$  mixing ratios, calculated from (a) the NOAA global latitudinal average marine boundary layer (gray) and the daily minimum measured at 483 m (black) and (b) the difference of these signals.

evaluated the wind errors for other locations, we note that the 3.6 m/s wind error used here is comparable to the mean wind error of 3.08 m/s, determined from radiosonde observations over the coterminous U.S. between 0 and 3 km in altitude [Lin and Gerbig, 2005].

[24] Uncertainty due to errors in modeled PBL heights  $\underline{S}_{TransPBL}$  is estimated by propagating the residual error  $Z_i$  into the predicted  $\text{CH}_4$  signals. Here we use the estimate of residual error in  $Z_i$  determined from the comparison between predicted WRF-STILT PBL height and PBL height measured with the wind profiler. The sensitivity of  $\text{CH}_4$  signal to  $Z_i$  is expressed as a first order perturbation in  $C$  as

$$\gamma = \frac{dC}{dZ_i} \quad (7)$$

where  $\gamma$  is estimated by calculating STILT footprints and then variations in  $C$  for small perturbations in  $Z_i$ . The error due to error in  $Z_i$  can then be estimated as

$$S_{TransPBL} = \frac{\Delta C}{\langle C \rangle} = \frac{\gamma \cdot \Delta Z_i}{\langle C \rangle} \quad (8)$$

where  $\Delta Z_i$  is the residual error in WRF-STILT  $Z_i$ , and  $\langle C \rangle$  is the mean total  $\text{CH}_4$  signal. Note that this error is calculated for well-mixed conditions. Using equations (7) and (8), the estimated transport error due to PBL uncertainties is 22% of the mean signal.

[25] The background error ( $\underline{S}_{bkgd}$ ) is due to the uncertainty in estimating the background contribution to the  $\text{CH}_4$  measurements at WGC 91 m. For this study, we estimate the upstream background  $\text{CH}_4$  mixing ratio using the final latitude of each particle as a lookup into the latitudinally averaged marine boundary layer (MBL)  $\text{CH}_4$  for October–December 2007 (NOAA Globalview  $\text{CH}_4$ ). Only time points (>95% of the total) for which more than 80% of the particles reached longitudes 1.5 degrees from the coast were included in the study. We expect that the NOAA MBL average will be a reasonable approximation for the  $\text{CH}_4$

background because it is heavily weighted to the Pacific and the typical  $\text{CH}_4$  gradients between Pacific and Atlantic are less than 10 ppb. We evaluated the error in  $\text{CH}_4$  background using the daily minimum  $\text{CH}_4$  mixing ratio measured at 483 m. The reason that the daily minimum  $\text{CH}_4$  mixing ratio at 483 m often reflects that of background air is because the 483 m sample height decouples from the surface at night (when  $91 \text{ m} < Z_i < 483 \text{ m}$ ) as indicated in Figure 1. A comparison of the  $\text{CH}_4$  mixing ratios determined from the NOAA MBL average and WGC 483 m minimum estimates is shown as a function of time in Figure 6. Figure 6b shows that there is no systematic bias, although the minimum  $\text{CH}_4$  mixing ratio at 483 m is occasionally enhanced relative to the NOAA MBL average, likely due to local  $\text{CH}_4$  contributions. We estimate the error due to  $\text{CH}_4$  background as the RMS difference in Figure 6b, which is 15% of the mean background-subtracted measurements at 91 m.

[26] The eddy flux error ( $\underline{S}_{eddy}$ ) specifies the fluctuations in  $\text{CH}_4$  mixing ratios due to contributions from turbulent eddies. Gerbig *et al.* [2003a] observed it is  $\sim 0.2$  ppm for  $\text{CO}_2$ . For  $\text{CH}_4$  studied here, a value of 1% is assumed. The error due to omitting ocean emissions ( $\underline{S}_{ocean}$ ) is assumed to be negligible. To evaluate this assumption, we calculated the expected  $\text{CH}_4$  signal from the Coal Point field near Santa Barbara, the largest known coastal natural gas field near California [Mau *et al.*, 2007], and found the signals to be less than 1 ppb.

[27] In order to combine the above errors from different sources, we need to know their correlations, which are unfortunately unknown. Assuming the errors from different sources are independent, the above errors are combined in quadrature to yield a total expected model prediction mismatch error of 32%.

### 3. Results

#### 3.1. $\text{CH}_4$ Mixing Ratios

[28] Predicted  $\text{CH}_4$  signals and background-subtracted measurements at 91 m are shown in Figure 7. As described

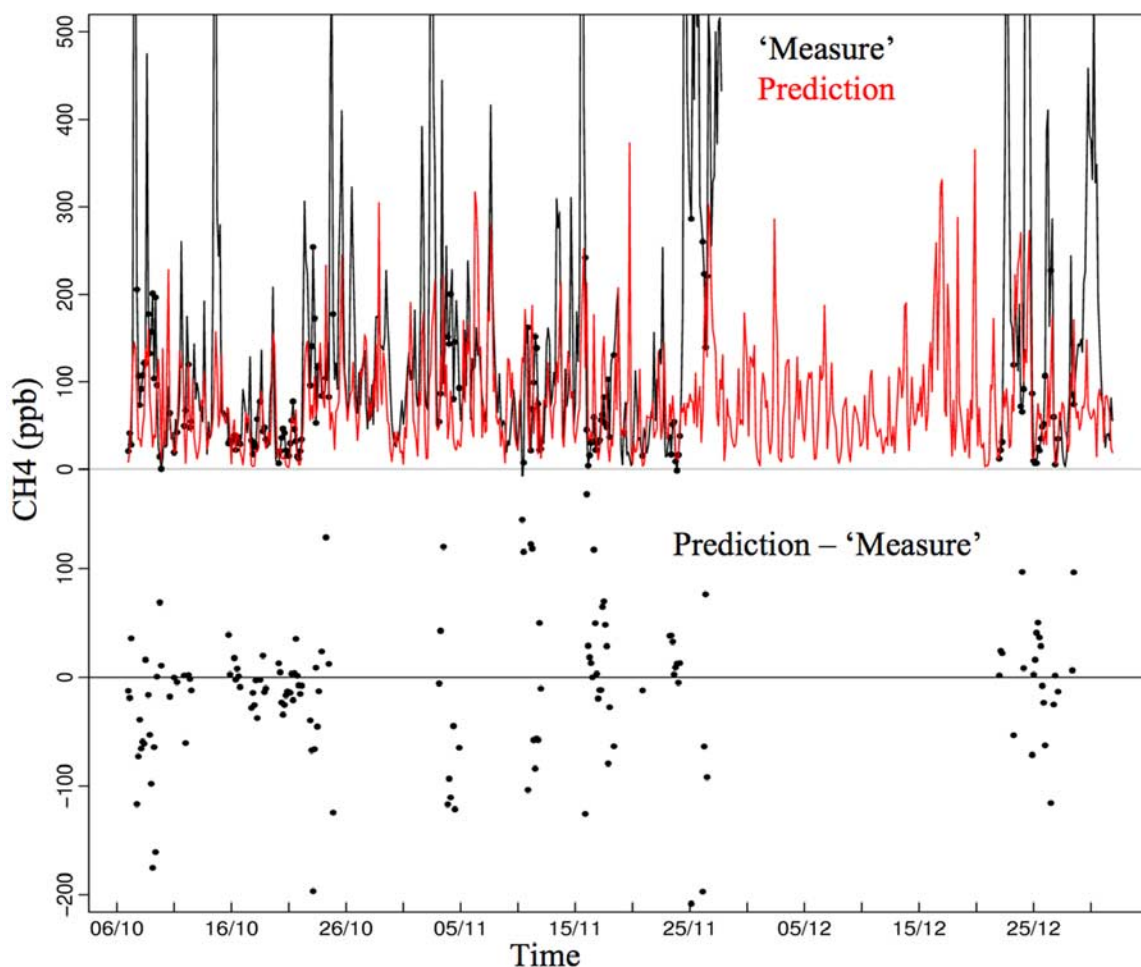


**Figure 7.** Background subtracted  $\text{CH}_4$  measurements (black line) and predictions (red line) from 91 m as (top) a function of time and (bottom) their difference for well-mixed conditions (black points).

in sections 2.1 and 2.8, data are selected to only include times with well-mixed conditions and when background  $\text{CH}_4$  can be reliably, which are shown as black points in Figure 7. Diurnal cycles due to changing boundary layer height and synoptic variations due to frontal passages are apparent in the data. The data gap in early–mid December resulted from a leak in the sampling system that was diagnosed and repaired. The measured and predicted  $\text{CH}_4$  mixing ratios show similar temporal variations, indicating partial success of the model. However, the predicted signals do not always capture the large  $\text{CH}_4$  measurements, indicating some combination of errors in the a priori emission model (e.g., spatial pattern or limited resolution) and atmospheric transport (e.g., wind fields, boundary layer height).

### 3.2. Inferred Surface Emissions

[29] We compare the tower measurements and WRF-STILT simulations at WGC site during winter (October–December) 2007. Three analyses are reported here: (1) a linear analysis for total  $\text{CH}_4$  emissions; (2) a “source analysis” for the six  $\text{CH}_4$  source sectors; and (3) a “region analysis” for thirteen regions in CA. For the linear analysis, we employ a Chi-square linear regression analysis by assuming equal relative errors of 32% in both variables.

For the “source analysis” and “region analysis,” the Bayesian analysis from equations (7) and (8) is applied. Note that the “region analysis” used the same a priori spatial distributions of  $\text{CH}_4$  emissions as the “source analysis,” and same total effective measurement errors of 32% are used in the following analyses.

#### 3.2.1. Linear Regression Analysis

[30] Results of the regression analyses using California specific emission applied to the October through December 2007 period are shown in Figures 8a and 8b. Without  $Z_i$  scaling (Figure 8a), the best fit slope between predicted and measured  $\text{CH}_4$  mixing ratios is  $0.46 \pm 0.07$ . After applying the  $Z_i$  scaling to WRF-STILT (Figure 8b), the slope between predicted and measured  $\text{CH}_4$  is  $0.73 \pm 0.11$ . The change in slope between Figure 8a and Figure 8b demonstrates that scaling the PBL heights affects the predicted  $\text{CH}_4$  signals, and any residual uncertainty in PBL height should be considered as a source of uncertainty in the Bayesian analyses that follow. After the  $Z_i$  scaling, the slope obtained in Figure 8b suggests that the actual emissions are higher than inventory estimates by a factor of  $1.37 \pm 0.21$ . We note that the normalized Chi-square value for Figure 8b is 1.17, suggesting that the estimated errors do not completely explain the residual variance in the differences between the predictions and measurements.  $\text{CH}_4$  signals based on

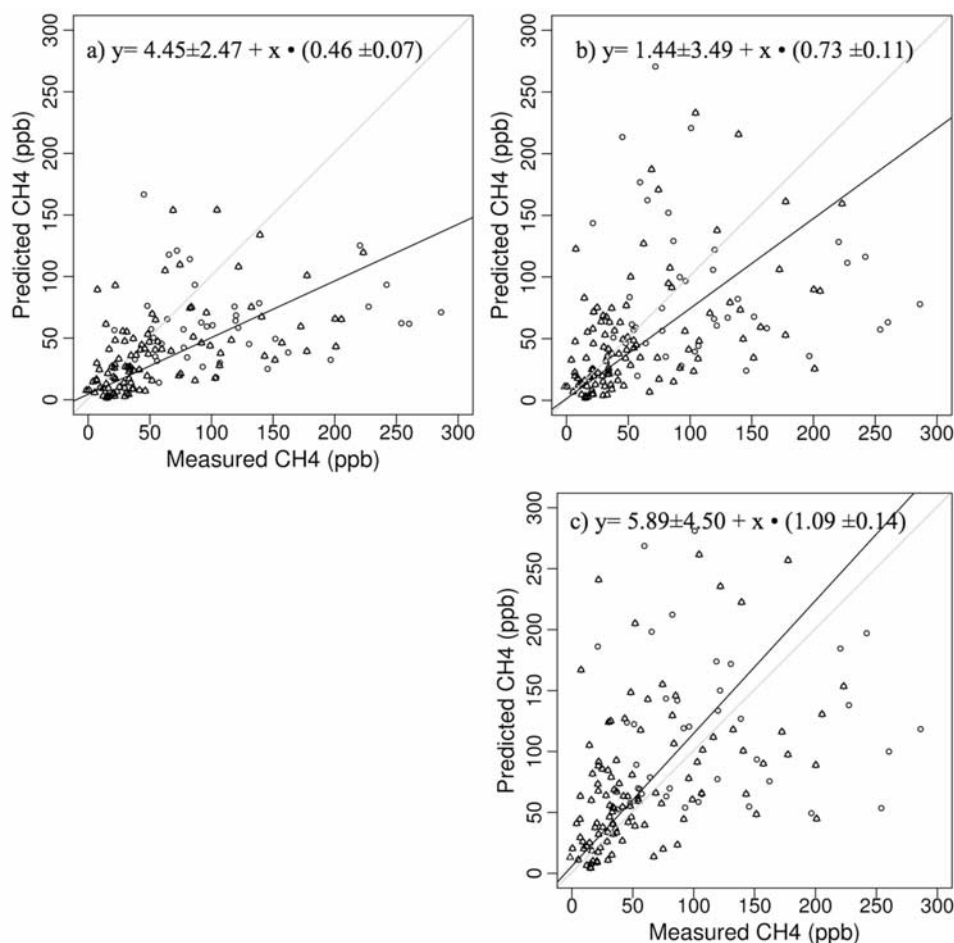


**Figure 8.** Predicted versus measured CH<sub>4</sub> obtained (a) using California specific emissions without *Zi* correction, (b) with *Zi* correction, and (c) using Edgar 3.2 emissions with *Zi* correction. The symbols indicate well-mixed periods when the difference between CH<sub>4</sub> mixing ratios measured at 91 and 483 m are less than 100 ppb (open circles) and less than 50 ppb (triangles), respectively.

Edgar 3.2 emissions are also simulated and compared with the tower measurements in Figure 8c, yielding a slope of  $1.09 \pm 0.14$ . This slope is roughly consistent ( $p > 0.1$  in a *t* test) with the slope ( $0.92 \pm 0.03$ ) obtained by Kort *et al.* [2008] in their comparison of measured and predicted CH<sub>4</sub> signals using Edgar 3.2. However, the slopes obtained with the California specific (Figure 8b) and Edgar (Figure 8c) emissions are significantly different ( $p < 0.01$ ), as might be expected given the large difference in the a priori emissions shown in Table 1. For the central California region, the total emission estimated by Edgar 3.2 is about 75% more than that estimated from California specific sources, which is roughly consistent with the difference ( $\sim 50\%$ ) of fitting slopes between Figure 8b and Figure 8c.

[31] To evaluate the effect of the well-mixed data selection criteria, we also examined the slopes obtained with a more stringent requirement that the difference between CH<sub>4</sub> mixing ratio measured at 91 m and 483 m is less than 50 ppb. This subset of data are shown as triangles in Figure 8. Using the selection criteria of 50 ppb in Figure 8 obtains a slope of  $0.86 \pm 0.17$ , which is quite consistent with that obtained using the selection criteria of 100 ppb. The following analyses include data based on the 100 ppb selection criteria.

### 3.2.2. Bayesian Analysis

[32] The Bayesian “source” inverse analysis was carried out for the six source sectors for October through December 2007. As shown in Figure 9a, the a posteriori scaling factors for the crop agriculture (CP), landfill (LF), wetland (WL), petroleum (PL), and natural gas (NG) are not significantly different from unity (at 95% confidence). The scaling factor for livestock is  $1.63 \pm 0.22$ , suggesting the emissions from livestock are significantly (95% confidence) larger than the a priori inventory estimates. The Bayesian “region” inverse analysis of emissions from the 13 California regions is shown in Figure 9b. The a posteriori uncertainties are noticeably reduced relative to the a priori uncertainties only for regions 6, 7, and 8, which have a strong influence on the CH<sub>4</sub> measurements either because the land surrounds the tower site (regions 6 and 8) or has a teleconnection through the prevailing wind (region 7). The a posteriori scaling factor for region 6 is  $1.08 \pm 0.06$ , indicating that the posterior emissions agree well with the a priori inventory estimates. Posterior scaling factors for region 7 and 8 are  $1.55 \pm 0.17$  and  $1.37 \pm 0.15$  respectively, indicating that the a posteriori emissions are greater than the a priori estimates for these two regions.

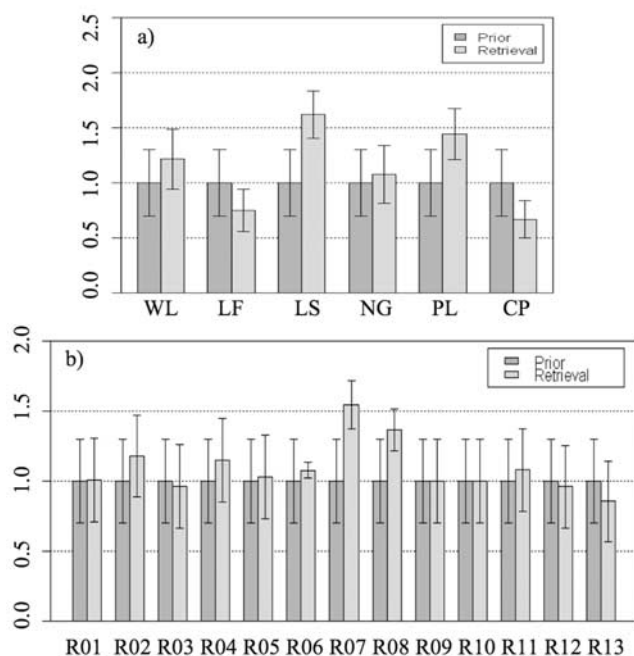


**Figure 9.** Inversion estimates for the (a) “source” sector analysis and (b) “region” analysis. A priori and posterior scaling factors for the six source sectors and 13 source regions are shown with corresponding 68% confidence level uncertainties.

[33] After applying the scaling factors obtained from Bayesian analyses, the posterior predicted  $\text{CH}_4$  mixing ratios are compared with measurements in Figure 10. Figure 10a shows the comparison for results from the “source analysis” with measurements. Compared to Figure 8b (before inverse optimization), the fitting slope is closer to unity, and the normalized Chi-square value is slightly reduced from 1.17 to 1.11. This suggests that the inverse optimization has slightly improved the agreement between the measured and predicted  $\text{CH}_4$  signals but that on order 10% of the variance remains unexplained. It is

possible that the apparent underestimation of the errors may be due to positive correlation between the error sources that we assumed independent. Similar results are obtained for the region analysis, as shown in Figure 10b. In both cases, the slopes after optimization are still slightly less than unity, likely because of the weight on the a priori scaling factors. We note that relaxing the a priori uncertainties on the scaling factors from 30% to 50%, allows the optimization to adjust the posterior scaling factors further from their a priori values.

#### 4. Discussion and Conclusions

[34] Here we discuss the impact of error in PBL height on uncertainty in estimated  $\text{CH}_4$  emissions, the implications of our results on estimated  $\text{CH}_4$  emissions from Central California, and conclude with recommendations for additional measurement sites that would help quantify  $\text{CH}_4$  emissions from more regions in California.

[35] First, the results of this work highlight the need for careful estimation and minimization of errors in the transport model. Our work is really only a first step in this regard because we have only evaluated wind and PBL height errors for one site, albeit at the location where the  $\text{CH}_4$  measurements were made. The comparison between the radar profiler measurements and WRF-STILT predictions of PBL height show a systematic overestimation in the WRF-STILT predictions, while the sensitivity test shows that predicted  $\text{CH}_4$  emission estimates are sensitive to PBL height. The error in WRF-STILT predictions of PBL height may be a result of imperfect land surface parameterization in WRF that does not account for a suppression of PBL height in the Central Valley. Possible causes for overestimation of PBL height include the Pacific low over California’s interior and low ratios of sensible to latent heat (Bowen ratios) driven by agricultural irrigation as shown in recent model studies of California [Kueppers *et al.*, 2007; Lobel and Bonfils, 2008]. Because of the limited amount of PBL height data, the present work should be considered a first step toward a more comprehensive analysis employing profiler data from additional profiler sites and over longer

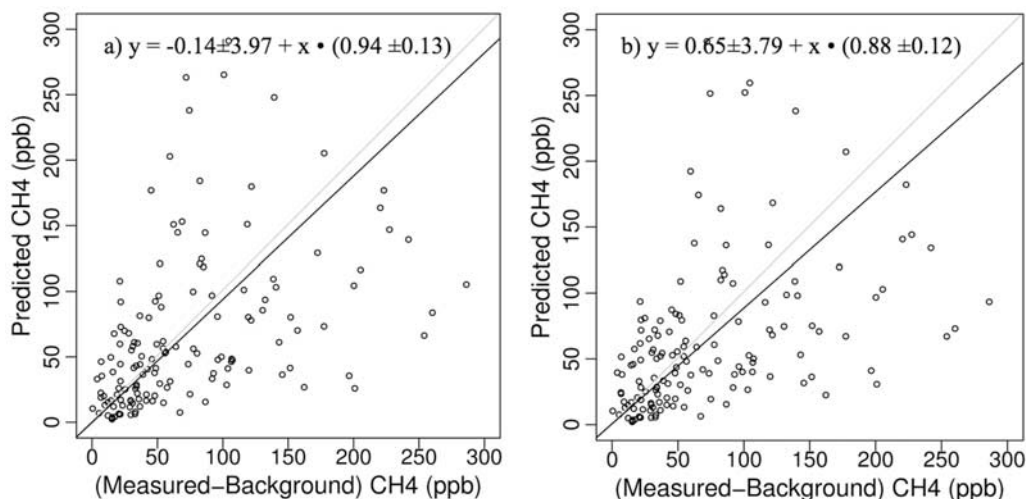


**Figure 10.** Comparison of  $\text{CH}_4$  mixing ratios between measurements and predictions modified using posterior scaling factors obtained from the (a) “source” analysis and (b) “region” analysis.

periods. We expect that this effort will substantially improve the fidelity of the WRF-STILT PBL predictions and hence accuracy of GHG emission inversions.

[36] Second, the linear regression estimates suggest that October–December CH<sub>4</sub> emissions from Central California are estimated to be  $37 \pm 21\%$  higher than the annually averaged California specific a priori inventories. Examining the source sector results, the increase in overall emissions is largely due to the  $63 \pm 22$  ( $1\sigma$ )% increase in estimated emissions from livestock. State-wide a priori livestock emission are 9.7 MMT CO<sub>2eq</sub> (see Table 1), which includes 5.6 MMT CO<sub>2eq</sub> from dairies and 4.1 MMT CO<sub>2eq</sub> from other cattle. Scaling the a priori CH<sub>4</sub> emissions from dairies suggests that actual dairy emissions are  $9.1 \pm 1.3$  MMT CO<sub>2eq</sub>. This result is nominally consistent with or slightly less than the results of a recent study by Salas *et al.* [2009], which estimated total CH<sub>4</sub> emissions from dairies in CA to be approximately 9.8 MMT CO<sub>2eq</sub>. We note that the source sector and regional analyses are consistent with each other in that CH<sub>4</sub> emission from region 8, which is dominated by livestock, shows a large and statistically significant increase relative to the a priori inventory. Some other sources also showed smaller but not significant differences from inventory estimates. For example, inferred CH<sub>4</sub> emissions from crop agriculture are smaller than the annually averaged inventory, consistent to the expectation of higher CH<sub>4</sub> emissions from the north-central Valley during the summer due to flooded rice agriculture [Salas *et al.*, 2006]. Finally, the “region” analysis shows that emissions from regions 6, 7 and 8 are constrained by the measurements. This is because they either surround the tower (i.e., regions 6 and 8) or have a strong influence on air reaching the tower through prevailing winds from the Bay Area to the Sacramento Valley (i.e., region 7). This observation provides an insight into the spatial domain that can be effectively investigated with the tower measurements and suggests that a network of towers would be required to accurately constrain the multiple regions and air basins in California. In principle, measurements from multiple towers would also be combined in a larger inverse analysis to provide more stringent constraints on emissions from regions that influence several towers. We consider a model-based design of a dedicated tower network to be a natural extension of the work described here.

[37] **Acknowledgments.** We thank Dave Field, Dave Bush, Edward Wahl, and particularly Jon Kofler for assistance with installation and maintenance of the instrumentation at WGC, Edward Dlugokencky for advice and assistance in verifying the Picarro instrument performance at NOAA, John Lin and Steve Wofsy for generously sharing the STILT code and providing expert advice, Chris Potter and William Salas for sharing their models of CH<sub>4</sub> emission for use as a priori estimates, Larry Hunsaker and Webster Tassat for providing the CARB estimates of landfill CH<sub>4</sub> emissions, Ken Massarie for providing the global CH<sub>4</sub> background data, and Susan James for assistance in running WRF on the LBNL-ASD computer cluster. We gratefully acknowledge NOAA Air Resources Laboratory (ARL) for the use of the HPSPLIT model underlying STILT and NCEP for the provision of the NARR meteorology. We also thank Jean Bogner, Nancy Brown, Eric Crosson, Guido Franco, Ling Jin, Ying-Kuang Hsu, Eileen McCauley, Tony VanCuren, James Wilczak, and three anonymous reviewers for valuable comments. This study was supported by the California Energy Commission (CEC) Public Interest Environmental Research Program and the Director, Office of Science, Office of Basic Energy Sciences of the U.S. Department of Energy under contract DE-AC02-05CH11231. The findings, views, and opinions presented in this paper do not necessarily represent the views and opinions of the California Energy Commission or the State of California.

## References

- Bergamaschi, P., M. Braunlich, T. Marik, and C. A. M. Brenninkmeijer (2000), Measurements of the carbon and hydrogen isotopes of atmospheric methane at Izana, Tenerife: Seasonal cycles and synoptic-scale variations, *J. Geophys. Res.*, **105**(D11), 14,531–14,546.
- Bergamaschi, P., M. Krol, F. Dentener, A. Vermeulen, F. Meinhardt, R. Graul, M. Ramonet, W. Peters, and E. J. Dlugokencky (2005), Inverse modeling of national and European CH<sub>4</sub> emissions using the atmospheric zoom model TM5, *Atmos. Chem. Phys.*, **5**, 2431–2460.
- Bergamaschi, P., *et al.* (2007), Satellite cartography of atmospheric methane from SCIAMACHY on board ENVISAT: 2. Evaluation based on inverse model simulations, *J. Geophys. Res.*, **112**, D02304, doi:10.1029/2006JD007268.
- Bianco, L., and J. M. Wilczak (2002), Convective boundary layer depth: Improved measurement by Doppler radar wind profiler using fuzzy logic methods, *J. Atmos. Ocean. Technol.*, **19**(11), 1745–1758.
- Bianco, L., J. M. Wilczak, and A. B. White (2008), Convective boundary layer depth estimation from wind profilers: Statistical comparison between an automated algorithm and expert estimations, *J. Atmos. Ocean. Tech.*, **25**, 1397–1413.
- CARB (2007), California 1990 Greenhouse Gas Emissions Level and 2020 Emissions Limit, California Air Resources Board Staff Report. (Available at [http://www.arb.ca.gov/cc/inventory/pubs/reports/staff\\_report\\_1990\\_level.pdf](http://www.arb.ca.gov/cc/inventory/pubs/reports/staff_report_1990_level.pdf))
- Carr, N. (2004), Overall Waste Stream Composition Data. California Integrated Waste Management Board: 1999 California Statewide Waste Disposal Characterization Study. (Available at <http://www.ciwm.ca.gov/WasteChar/Study1999/OverTabl.htm>)
- Census of Agriculture (2002), Volume 1 California County Level Data. National Agricultural Statistical Services for U.S. Agriculture Statistical Information and Graphs, United States Department of Agriculture. (Available at <http://www.nass.usda.gov/census/census02/volume1/ca/index2.htm>)
- Chen, Y.-H., and R. G. Prinn (2006), Estimation of atmospheric methane emissions between 1996 and 2001 using a three-dimensional global chemical transport model, *J. Geophys. Res.*, **111**, D10307, doi:10.1029/2005JD006058.
- Chen, S.-H., and W.-Y. Sun (2002), A one-dimensional time dependent cloud model, *J. Meteorol. Soc. Jpn.*, **80**, 99–118.
- Chou, M.-D., and M. J. Suarez (1994), An efficient thermal infrared radiation parameterization for use in general circulation models, *NASA/TM-104606*, 84 pp., NASA Tech. Memo.
- Dentener, F., W. Peters, M. Krol, M. van Weele, P. Bergamaschi, and J. Lelieveld (2003), Inter-annual-variability and trend of CH<sub>4</sub> lifetime as a measure for OH changes in the 1979–1993 time period, *J. Geophys. Res.*, **108**(D15), 4442, doi:10.1029/2002JD002916.
- Dye, T. S., C. G. Lindsey, and J. A. Anderson (1995), Estimates of mixing depth from “boundary layer” radar profilers, *Preprints from the 9th Symposium on Meteorological Observations and Instrumentation*, Charlotte, N. C., March 27–31, pp. 156–160, (STI-94212-1451).
- Farrell, A., A. C. Kerr, A. R. Brandt, M. S. Torn, and G. Franco (2005), Research Roadmap for Greenhouse Gas Inventory Methods. California Energy Commission: Public Interest Energy Research, (CEC-500-2005-097).
- Franco, G. (2002), Inventory of California Greenhouse Gas Emissions and Sinks: 1990–1999. California Energy Commission: Public Interest Energy Research, (CEC-600-02-001F).
- Gerbig, C., J. C. Lin, S. C. Wofsy, B. C. Daube, A. E. Andrews, B. B. Stephens, P. S. Bakwin, and C. A. Grainger (2003a), Toward constraining regional-scale fluxes of CO<sub>2</sub> with atmospheric observations over a continent: 1. Observed spatial variability from airborne platforms, *J. Geophys. Res.*, **108**(D24), 4756, doi:10.1029/2002JD003018.
- Gerbig, C., J. C. Lin, S. C. Wofsy, B. C. Daube, A. E. Andrews, B. B. Stephens, P. S. Bakwin, and C. A. Grainger (2003b), Toward constraining regional-scale fluxes of CO<sub>2</sub> with atmospheric observations over a continent: 2. Analysis of COBRA data using a receptor-oriented framework, *J. Geophys. Res.*, **108**(D24), 4757, doi:10.1029/2003JD003770.
- Gimson, N. R., and M. Uliasz (2003), The determination of agricultural methane emissions in New Zealand using receptor-oriented modelling techniques, *Atmos. Environ.*, **37**, 3903–3912.
- Grell, G. A., and D. Devenyi (2002), A generalized approach to parameterizing convection combining ensemble and data assimilation techniques, *Geophys. Res. Lett.*, **29**(14), 1693, doi:10.1029/2002GL015311.
- Hansen, J. (2004), Defusing the global warming time bomb, *Sci. Am.*, **290**(3), 68–77.
- Hansen, J., M. Sato, J. Glasco, and R. Ruedy (1998), A common sense climate index: Is climate changing noticeably?, *Proc. Natl. Acad. Sci.*, **95**, 4113–4120.

- Harriss, R. C. (1994), Reducing urban sources of methane: An experiment in industrial ecology, in *Industrial Ecology and Global Change*, pp. 223–238, Cambridge Univ. Press, New York.
- Hein, R., P. J. Crutzen, and M. Heimann (1997), An inverse modeling approach to investigate the global atmospheric methane cycle, *Global Biogeochem. Cycles*, 11(1), 43–76.
- Hofman, D. J., J. H. Butler, E. J. Dlugokencky, J. W. Elkins, K. Masarie, S. A. Montzka, and P. Tans (2006), The role of carbon dioxide in climate forcing from 1979–2004: Introduction of the Annual Greenhouse Gas Index, *Tellus B*, 58B, 614–619.
- Houweling, S., T. Kaminski, F. Dentener, J. Lelieveld, and M. Heimann (1999), Inverse modeling of methane sources and sinks using the adjoint of a global transport model, *J. Geophys. Res.*, 104(D21), 26,137–26,160.
- Houweling, S., T. Röckmann, I. Aben, F. Keppler, M. Krol, J. F. Meirink, E. J. Dlugokencky, and C. Frankenberg (2006), Atmospheric constraints on global emissions of methane from plants, *Geophys. Res. Lett.*, 33, L15821, doi:10.1029/2006GL026162.
- IPCC (2006), Guidelines for National Greenhouse Gas Inventories. (Available at <http://www.ipcc-nggip.iges.or.jp/public/2006gl/index.htm>)
- IPCC (2007), *IPCC Fourth Assessment Report (AR4)*, “Climate Change 2007: Impacts, Adaptation and Vulnerability”, Cambridge Univ. Press, New York.
- Kaminski, T., P. J. Rayner, M. Heimann, and I. G. Enting (2001), On aggregation errors in atmospheric transport inversions, *J. Geophys. Res.*, 106(D5), 4703–4715.
- Kort, E. A., J. Eluszkiewicz, B. B. Stephens, J. B. Miller, C. Gerbig, T. Nehrkorn, B. C. Daube, J. O. Kaplan, S. Houweling, and S. C. Wofsy (2008), Emissions of CH<sub>4</sub> and N<sub>2</sub>O over the United States and Canada based on a receptor-oriented modeling framework and COBRA-NA atmospheric observations, *Geophys. Res. Lett.*, 35, L18808, doi:10.1029/2008GL034031.
- Kueppers, L. M., M. A. Snyder, and L. C. Sloan (2007), Irrigation cooling effect: Regional climate forcing by land-use change, *Geophys. Res. Lett.*, 34, L03703, doi:10.1029/2006GL028679.
- Lelieveld, J., P. J. Crutzen, and F. J. Dentener (1998), Changing concentration, lifetime, and climate forcing of atmospheric methane, *Tellus B*, 50, 128–150.
- Lin, J. C., and C. Gerbig (2005), Accounting for the effect of transport errors on tracer inversions, *Geophys. Res. Lett.*, 32, L01802, doi:10.1029/2004GL021127.
- Lin, Y.-L., R. D. Farley, and H. D. Orville (1983), Bulk parameterization of the snow field in a cloud model, *J. Appl. Meteorol.*, 22, 1065–1092.
- Lin, J. C., C. Gerbig, S. C. Wofsy, A. E. Andrews, B. C. Daube, K. J. Davis, and C. A. Grainger (2003), A near-field tool for simulating the upstream influence of atmospheric observations: The Stochastic Time-Inverted Lagrangian Transport (STILT) model, *J. Geophys. Res.*, 108(D16), 4493, doi:10.1029/2002JD003161.
- Lin, J. C., C. Gerbig, S. C. Wofsy, A. E. Andrews, B. C. Daube, C. A. Brainger, B. B. Stephens, P. S. Bakwin, and D. Y. Hollinger (2004), Measuring fluxes of trace gases at regional scales by Lagrangian observations: Application to the CO<sub>2</sub> Budget and Rectification Airborne (COBRA) study, *J. Geophys. Res.*, 109, D15304, doi:10.1029/2004JD004754.
- Lobel, D. B., and C. Bonfils (2008), The effect of irrigation on regional temperatures: A spatial and temporal analysis of trends in California, 1934–2002, *J. Clim.*, 21, 2063.
- Manning, A. J., D. B. Ryall, R. G. Derwent, P. G. Simmonds, and S. O’Doherty (2003), Estimating European emissions of ozone-depleting and greenhouse gases using observations and a modeling back-attribution technique, *J. Geophys. Res.*, 108(D14), 4405, doi:10.1029/2002JD002312.
- Matross, D. M., et al. (2006), Estimating regional carbon exchange in New England and Quebec by combining atmospheric, ground-based and satellite data, *Tellus B*, 58, 344–358.
- Mau, S., D. L. Valentine, J. F. Clark, J. Reed, R. Camilli, and L. Washburn (2007), Dissolved methane distributions and air-sea flux in the plume of a massive seep field, Coal Oil Point, California, *Geophys. Res. Lett.*, 34, L22603, doi:10.1029/2007GL031344.
- Mesinger, F., et al. (2006), North American regional reanalysis, *Bull. Am. Meteorol. Soc.*, 87(3), 343–360.
- Mikaloff Fletcher, S. E., P. P. Tans, L. M. Bruhwiler, J. B. Miller, and M. Heimann (2004a), CH<sub>4</sub> sources estimated from atmospheric observations of CH<sub>4</sub> and its 13C/12C isotopic ratios: 1. Inverse modeling of source processes, *Global Biogeochem. Cycles*, 18, GB4005, doi:10.1029/2004GB002223.
- Mikaloff Fletcher, S. E., P. P. Tans, L. M. Bruhwiler, J. B. Miller, and M. Heimann (2004b), CH<sub>4</sub> sources estimated from atmospheric observations of CH<sub>4</sub> and its 13C/12C isotopic ratios: 2. Inverse modeling of CH<sub>4</sub> fluxes from geographical regions, *Global Biogeochem. Cycles*, 18, GB4005, doi:10.1029/2004GB002224.
- Miller, J. B., and P. P. Tans (2003), Calculating isotopic fractionation from atmospheric measurements at various scales, *Tellus B*, 55(2), 207–214.
- Miller, S. M., et al. (2008), Sources of carbon monoxide and formaldehyde in North America determined from high-resolution atmospheric data, *Atmos. Chem. Phys.*, 8, 7673–7696.
- Mlawer, E. J., S. J. Taubman, P. D. Brown, M. J. Iacona, and S. A. Clough (1997), Radiative transfer for inhomogeneous atmospheres: RRTM, a validated correlated-k model for the longwave, *J. Geophys. Res.*, 102(D14), 16,663–16,682.
- Olivier, J. G. J., J. A. Van Aardenne, F. Dentener, L. Ganzeveld, and J. A. H. W. Peters (2005), Recent trends in global greenhouse gas emissions: Regional trends and spatial distribution of key sources, in *Non-CO<sub>2</sub> Greenhouse Gases (NGGG-4)*, pp. 325–330, Millpress, Rotterdam, Netherlands.
- Potter, C., S. Klooster, S. Hiatt, M. Fladeland, V. Genovese, and P. Gross (2006), Methane emissions from natural wetlands in the United States: Satellite-derived estimation based on ecosystem carbon cycling, *Earth Interact.*, 10(22), 1–12.
- Salas, W., P. Green, S. Frolking, C. Li, and S. Boles (2006), Estimating Irrigation Water Use for California Agriculture: 1950s to Present. California Energy Commission, PIER Energy-Related Environmental Research, (CEC-500-2006-057).
- Salas, W., C. Li, F. Mitloehner, and J. Pisano (2009), Developing and Applying Process-based Models for Estimating GHG and Air Emission from California Dairies. California Energy Commission, PIER Energy-Related Environmental Research, (CEC-500-2008-093).
- Skamarock, W. C., J. B. Klemp, J. Dudhia, D. O. Gill, D. M. Barker, W. Wang, and J. G. Powers (2005), A description of the advanced research WRF version 2, *Tech. Note 468+STR*, 88 pp., MMM Division, NCAR, Boulder, Colo.
- Shindell, D. T., G. Faluvegi, N. Bell, and G. A. Schmidt (2005), An emissions based view of climate forcing by methane and tropospheric ozone, *Geophys. Res. Lett.*, 32, L04803, doi:10.1029/2004GL021900.
- USEPA (2004), *Inventory of U.S. Greenhouse Gas Emissions and Sinks: 1990–2002*, U.S. Environmental Protection Agency, Washington, D. C., April 15.
- Vermeulen, A. T., R. Eisma, A. Hensen, and J. Slanina (1999), Transport model calculations of NW-European methane emissions, *Environ. Sci. Policy*, 2, 315–324.
- Wyngaard, J. C., and M. A. LeMone (1980), Behavior of the refractive index structure parameter in the entraining convective boundary layer, *J. Atmos. Sci.*, 37, 1573–1585.

A. E. Andrews, L. Bianco, and A. Hirsch, Earth System Research Laboratory, NOAA, 325 Broadway R/GMD 1, Boulder, CO 80305, USA.  
 J. Eluszkiewicz and T. Nehrkorn, Atmospheric and Environmental Research, Inc., 131 Hartwell Avenue, Lexington, MA 02421-3126, USA.  
 M. L. Fischer and C. Zhao, Environmental Energy Technology Division, Lawrence Berkeley National Laboratory, MS 90K, 1 Cyclotron Road, Berkeley, CA 94720, USA. (czhao@lbl.gov)  
 C. MacDonald, Meteorological Measurements and Analysis, Sonoma Technology, Inc., 1455 N. McDowell Boulevard, Suite D, Petaluma, CA 94954, USA.